

Article

Effect of Low-Temperature Sensitization on Hydrogen Embrittlement of 301 Stainless Steel

Chieh Yu ^{1,†}, Ren-Kae Shiue ¹, Chun Chen ¹ and Leu-Wen Tsay ^{2,*}

¹ Department of Materials Science and Engineering, National Taiwan University, Taipei 106, Taiwan; d02527001@ntu.edu.tw (C.Y.); rkshiue@ntu.edu.tw (R.-K.S.); gchen@ntu.edu.tw (C.C.)

² Institute of Materials Engineering, National Taiwan Ocean University, Keelung 20224, Taiwan

* Correspondence: b0186@mail.ntou.edu.tw; Tel.: +886-2-2462-5324

† Current Address: National Chung-Shan Institute of Science and Technology, Materials & Electro-Optics Research Division, Lung-Tan, Tao-Yuan 325, Taiwan.

Academic Editor: Robert Tuttle

Received: 7 January 2017; Accepted: 10 February 2017; Published: 15 February 2017

Abstract: The effect of metastable austenite on the hydrogen embrittlement (HE) of cold-rolled (30% reduction in thickness) 301 stainless steel (SS) was investigated. Cold-rolled (CR) specimens were hydrogen-charged in an autoclave at 300 or 450 °C under a pressure of 10 MPa for 160 h before tensile tests. Both ordinary and notched tensile tests were performed in air to measure the tensile properties of the non-charged and charged specimens. The results indicated that cold rolling caused the transformation of austenite into α' and ϵ -martensite in the 301 SS. Aging at 450 °C enhanced the precipitation of $M_{23}C_6$ carbides, G, and σ phases in the cold-rolled specimen. In addition, the formation of α' martensite and $M_{23}C_6$ carbides along the grain boundaries increased the HE susceptibility and low-temperature sensitization of the 450 °C-aged 301 SS. In contrast, the grain boundary α' -martensite and $M_{23}C_6$ carbides were not observed in the as-rolled and 300 °C-aged specimens.

Keywords: stainless steel; hydrogen embrittlement; hydrogen charging; G and σ phases; α' martensite

1. Introduction

Austenitic stainless steels (SSs) have been extensively used in industrial applications due to their good combination of corrosion resistance and mechanical properties. Metastable austenitic SSs may undergo phase transformation from austenite (γ) into ferromagnetic α' -martensite during plastic deformation [1–5]. The induced martensite during tensile tests at room temperature enhances the elongation to fracture, hardness, and tensile strength [5]. However, the induced martensite increases the susceptibility of austenitic stainless steels to hydrogen embrittlement (HE) [2–8]. In hydrogen-containing environments, the more austenite transforms into martensite, the more ductility loss of the material occurs [6]. Hydrogen suppresses the transformation of austenite to martensite, leading to hydrogen softening and localized brittle fracture [5]. Moreover, the suppressed formation of α' -martensite in the highly strained region of a 304L specimen at 80 °C accounts for its lowered HE susceptibility [7]. It has been reported that strain-induced α' -martensite acts as a “hydrogen diffusion highway” in hydrogen-charged 304 SS [8], resulting in an increased hydrogen concentration at the crack tip and accelerated crack growth.

Austenitic stainless steels are susceptible to stress corrosion cracking (SCC) in chloride-containing solutions [9–15]. In $MgCl_2$ solution, the mechanism of environment-induced cracking of austenitic stainless steels can be either SCC or HE, depending on the test temperature [10,11]. A suitable amount of cold work can lower the SCC susceptibility of austenitic stainless steels, whereas excessive

cold working reverses that trend [16,17]. The machined 304L SS showed a marked increase in SCC susceptibility as compared with the solution-annealed, unmachined, and cold worked samples [18,19]. Unlike martensite-free 304 SS, 304 SS with machining-induced martensite is greatly embrittled and undergoes premature failure in 40 MPa hydrogen [20].

As austenitic stainless steels are heated in the temperature range between 500 °C and 850 °C, chromium carbides form along the grain boundary, leaving an adjacent chromium depletion zone. This phenomenon is called sensitization and it is responsible for intergranular corrosion or intergranular SCC (IGSCC) [21–24]. Cold-working austenitic stainless steels accelerates carbide precipitation, even in a Ti-stabilized (AISI 321) SS [24]. Cathodic hydrogen-charging greatly reduces the ductility of tensile specimens and decreases the time-to-failure of 304L SS and 308L weld metals under constant load tests, especially for the sensitized 304L (650 °C/24 h aging) [22]. Furthermore, the nucleation of tiny carbides in many austenitic SSs is enhanced by welding, thermo-mechanical processing, or slow cooling from the solution-annealed temperature. Such thermo or thermo-mechanical processes might not immediately induce IGSCC of the alloys. The number of carbide precipitates remains unchanged, but they grow in size during subsequent long-term service below 500 °C. Sensitization of austenitic SSs at temperatures below the classic sensitization range (500 °C–800 °C) is referred to as low-temperature sensitization (LTS).

Cold deformation increases the degree of 304 SS sensitization up to 65 times that of undeformed 304 SS tested at 500 °C [25]. In a previous study, 304 SS welds exposed to a temperature of 450 °C for 6600 h suffered from IGSCC due to the presence of $(\text{Fe,Cr})_{23}\text{C}_6$ carbides along grain boundaries [26]. Cold working of the steel increases the sensitization kinetics of austenitic SSs by up to 15%, while further cold working shows less effect on sensitization [23]. The induced martensite in cold-worked 304 [27] or 304L [28] SSs causes low-temperature sensitization at 380 °C [27] and 500 °C [28], thereby increasing the SCC susceptibility in a BWR (boiling water reactor) simulated environment [28]. Furthermore, sensitization causes α' -martensite transformation preferentially along the grain boundaries of 304 and 316 SSs, which provides a high diffusivity path of hydrogen to the crack tip [29] and enhances the intergranular fracture and HE susceptibility of the steel [29].

In this study, cold-rolled 301 SS was hydrogen-charged in an autoclave at 300 °C or 450 °C at the pressure of 10 MPa for 160 h before straining. The effects of low-temperature sensitization during aging/hydrogen-charging at 300 °C or 450 °C on the microstructure were investigated. The HE susceptibility of various specimens was correlated with the corresponding microstructures, particularly the induced martensite and fine precipitates in the specimens.

2. Experimental Procedures

The chemical composition of the AISI 301 SS used in this study was 16.71 Cr, 6.89 Ni, 0.08 C, 1.16 Mn, 0.54 Si, 0.02 P, 0.003 S, and the balance Fe in wt %. The 301 SS in the plate form with a thickness of 4.5 mm was solution-annealed at 1050 °C for 30 min and had a hardness of Hv 176. Cold rolling of the 301 SS plate with 30 % in thickness reduction was performed at room temperature, and designated as CR (cold-rolled) specimen. For comparison, CR specimens were aged at 300 °C or 450 °C for 160 h, and these specimens were respectively designated as CR-300 and CR-450.

Figure 1 shows the dimensions of the double-edge notched tensile and standard tensile specimens, which had a thickness of 3 mm. Cold-rolled specimens were hydrogen-charged in an autoclave at 300 °C or 450 °C at a pressure of 10 MPa for 160 h before straining. They were designated as CR-300H and CR-450H, respectively. Standard tensile specimens, according to ASTM E8 specification with a gauge length of 25 mm, were wire-cut directly from the cold-rolled plates along the rolling direction. Ordinary tensile tests were carried out at a strain rate of $6 \times 10^{-4} \text{ s}^{-1}$ (crosshead displacement rate of 0.9 mm/min) in laboratory air to determine the tensile properties of the non-hydrogen-charged specimens. Notched tensile tests were performed to evaluate the HE susceptibility of the hydrogen-charged specimens at a crosshead displacement rate of 0.72 mm/min at room temperature.

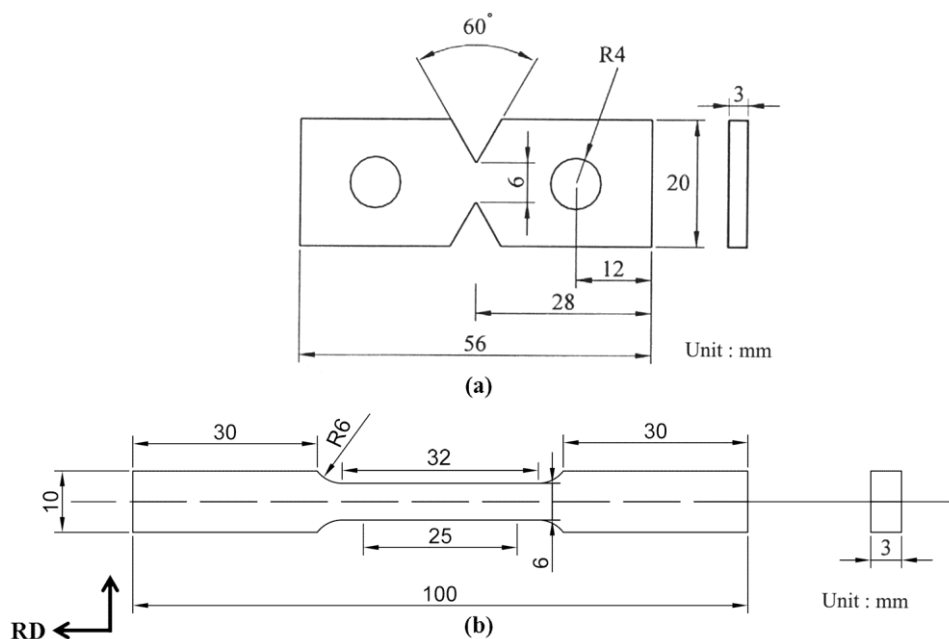


Figure 1. Schematic dimensions of (a) a double-edge notched specimen and (b) a standard tensile specimen. (RD: Rolling Direction).

A Fischer MP30 ferritescope (Windsor, CT, USA) can measure the ferrite contents precisely in austenitic and duplex SSs. The ferritescope was used in this study to determine the amounts of strain-induced α' -martensite in all specimens [30,31]. The hydrogen-charged samples (CR-300H and CR-450H) with the dimensions of $1 \times 1 \times 1 \text{ cm}^3$ were ground by No. 2000 SiC paper before cleaning. The hydrogen contents of the charged samples (CR-300H and CR-450H) were measured by using the LECO-TCH 600 (Saint Joseph, MI, USA). After hydrogen-charging, they were melted in a crucible. The amounts of H and O were calculated from the H_2O , CO, and CO_2 mixture. Fractographs of each specimen after tensile straining were inspected with a NOVA-450 scanning electron microscope (SEM, Hillsboro, OR, USA). Selected specimens were inspected by using a JEOL 2000EX transmission electron microscope (TEM, Akishima, Japan). A high resolution TEM (HRTEM), FEI Tecnai G2 F20 (Hillsboro, OR, USA), was applied to inspect the nano-sized precipitates in the specimen.

3. Results

3.1. Microstructural Observation

Figure 2 shows optical metallographs of cold-rolled specimens with different aging conditions. Figure 2a is a composite photograph of the CR specimen revealing the microstructures along three perpendicular directions. No severe texture was observed in the CR specimen after 30% thickness reduction. The CR specimen contained basket-weaved slip bands within equiaxial austenite grains. In the case of the specimens aged at 300 (CR-300) and 450 °C (CR-450), slip bands could be still observed clearly, as shown in Figure 2b,c. The ferritescope was used to determine the amount of strain-induced α' martensite formed in the tested specimens. The ferrite contents of the CR, CR-300, and CR-450 specimens were 26%, 26%, and 29%, respectively. It is well known that heating strain-induced α' martensite to an appropriate temperature will cause it to revert into austenite, leading to a decrease in ferrite content. It was deduced that increased amount of α' martensite in the CR-450 specimen was associated with a specific phase transformation in the specimen.

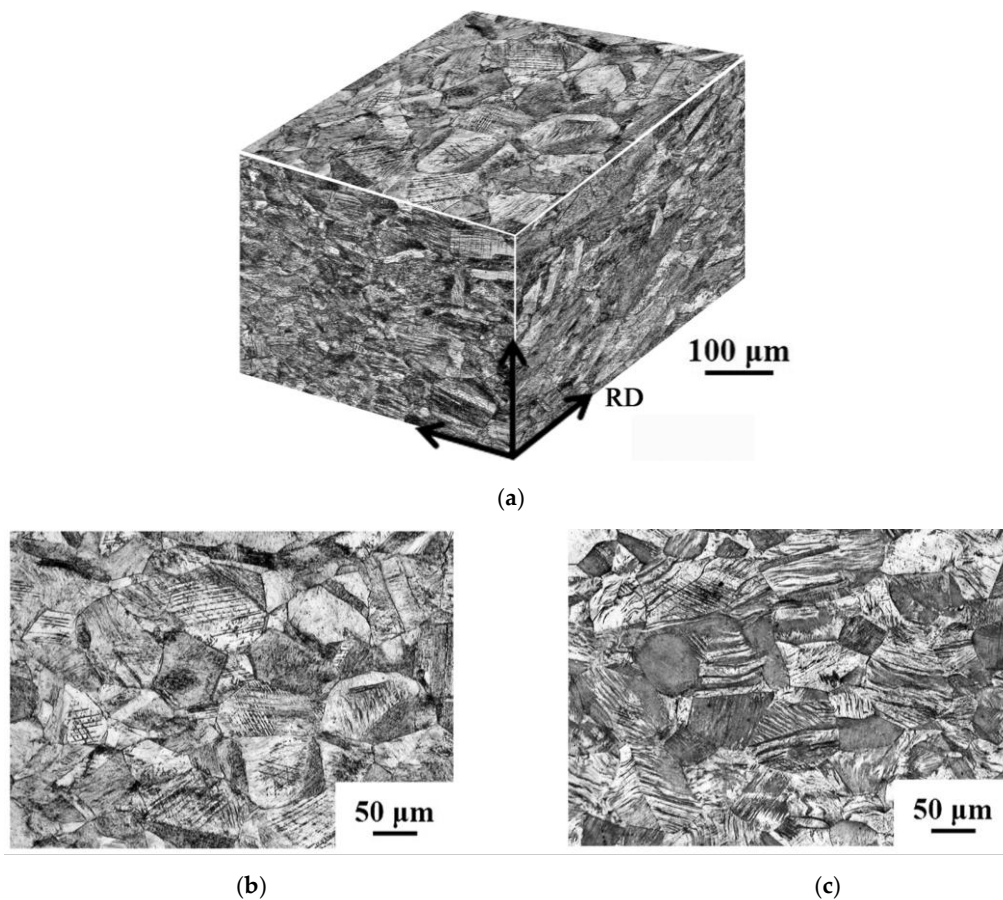


Figure 2. Optical metallographs of: (a) three mutually perpendicular planes of the CR, (b) CR-300, and (c) CR-450 specimens.

3.2. Mechanical Properties

Table 1 lists the mechanical properties of the test specimens. The 30% cold rolling obviously increased the surface hardness of CR specimen to Hv 455, as compared with the Hv 176 of the annealed 301 SS. Dislocation recovery during aging at 300 °C was expected to be responsible for the slight decrease in surface hardness of CR-300 specimen to Hv 445. The surface hardness of CR-450 specimen further reduced to Hv 414 due to the overage at 450 °C. The results of ordinary tensile tests revealed that all three tested specimens had the same elongation of 24%. The ordinary tensile strengths of the CR and CR-300 specimens were similar. However, the YS and UTS of the CR-450 specimen were lower than those of the CR and CR-300 ones.

Table 1. Mechanical properties of tested specimens with 30% reduction in thickness.

Specimen	YS ^a (MPa)	UTS ^b (MPa)	EL ^c (%)	Hardness(Hv)	NTS ^d (MPa)
CR	1350	1506	24	455	1737
CR-300 ^e	1400	1544	24	445	1743
CR-450 ^f	1200	1296	24	414	1584
CR-300H ^g	-	-	-	-	1339
CR-450H ^h	-	-	-	-	843

^a YS: offset yield strength; ^b UTS: ultimate tensile strength; ^c EL: elongation; ^d NTS: notched tensile strength; ^e CR-300: CR specimen aged at 300 °C for 160 h in vacuum; ^f CR-450: CR specimen aged at 450 °C for 160 h in vacuum; ^g CR-300H: CR specimen hydrogen-charged at 300 °C for 160 h; ^h CR-450H: CR specimen hydrogen-charged at 450 °C for 160 h.

Notched tensile tests were performed in air to evaluate the notch brittleness of the specimens. The NTSs of the CR, CR-300, and CR-450 specimens were 1737, 1743, and 1584 MPa, respectively. The NTS of the CR-450 specimen was lower than those of the CR and CR-300 ones. This is consistent with the YS and UTS results for the CR, CR-300, and CR-450 specimens. It is noted that the NTS was significantly higher than the corresponding UTS for all specimens, indicating that the notched specimens possessed enough toughness to resist localized brittle fracture before rupture in air.

Notched tensile strengths tested in air versus displacement curves of the non-charged (solid lines) and hydrogen-charged (dotted lines) specimens are shown in Figure 3. The NTSs of the CR and CR-300 specimens were similar, but the CR-300 specimen had a slightly higher notch displacement (notch ductility) than the CR one. In contrast, the NTS and notch displacement of the CR-450 specimen were obviously lower than those of the CR and CR-300 ones tested in air. Subsequently, aging the cold-rolled 301 SS at 450 °C was found to deteriorate its notched tensile properties. As shown in Figure 3, hydrogen-charging caused a significant drop in NTSs and notch displacements of both the CR-300H and CR-450H specimens. HE was responsible for such a severe degradation of notch tensile properties of the hydrogen-charged specimens. The results also indicated that the CR-450H specimen was more damaged by hydrogen-charging than the CR-300H one. Aging the cold worked specimen at higher temperature was expected to improve its ductility and reduce brittleness, but these improvements did not occur in the CR-450 specimen. This result would be addressed in the later discussion of the mechanism of deterioration in CR-450.

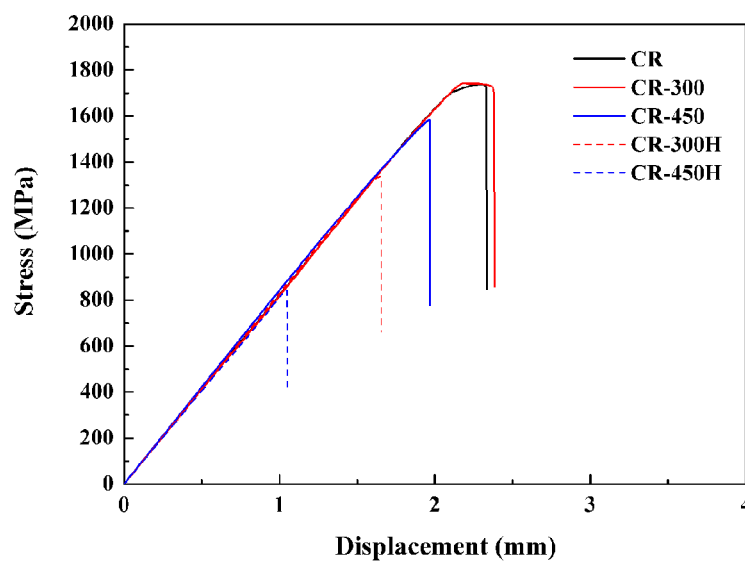


Figure 3. Notched tensile tests of non-hydrogen-charged (solid lines) and hydrogen-charged (dash lines) specimens.

3.3. Fractographic Examinations

The macroscopic fracture appearances of selected notched tensile specimens are shown in Figure 4. The fractographs of the CR and CR-300 specimens were alike, comprising extensive shear fractured (SF) regions (shear lips) on the lateral surfaces and triangular flat fracture (FF) zones ahead of the notch fronts, as shown in Figure 4a. A noticeable reduction of the SF regions and an increase in the size of the FF zone were observed in the CR-450 specimen after the notched tensile test (Figure 4b). Moreover, the fractograph shown in Figure 4b exhibited lamellar tears and many fine secondary cracks. Even without hydrogen-charging, the CR-450 specimen showed inherent notch brittleness in comparison with the CR and CR-300 specimens.

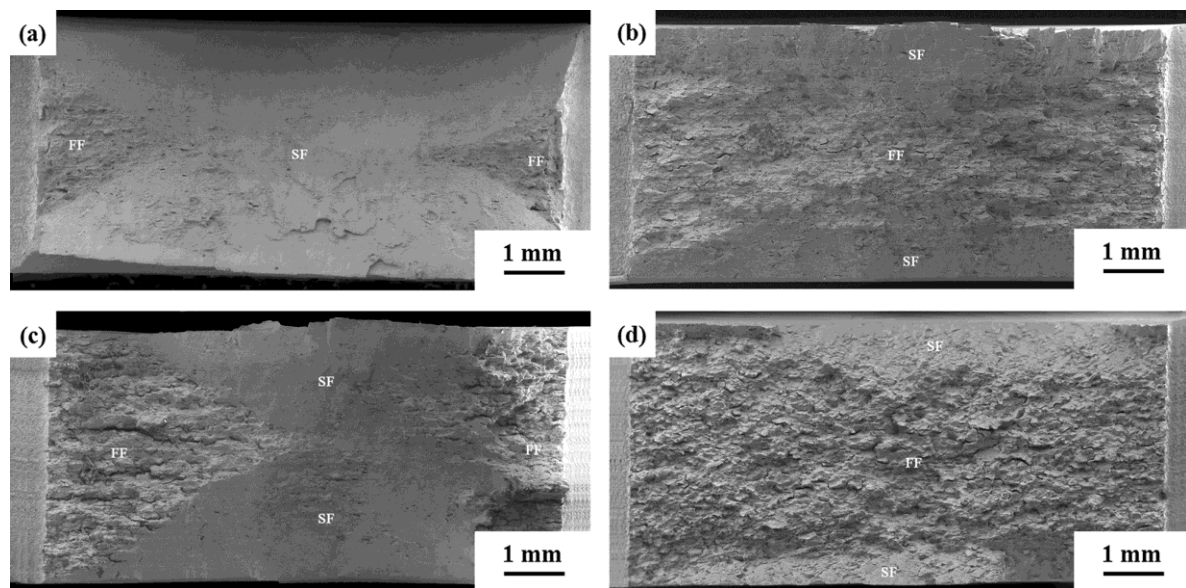


Figure 4. Macro-fracture appearances of (a) CR-300, (b) CR-450, (c) CR-300H, and (d) CR-450H specimens.

It is known that hydrogen tends to accumulate and embrittle the elastic-plastic boundaries of high-strength steels [32], and this embrittlement becomes more severe at the locations of stress concentration, such as a notch [33,34]. Moreover, a notch can produce a triaxial stress state, and limits the plastic deformation ahead of the notch tip. The marked decreases in NTSs and notch displacements of the hydrogen-charged specimens (CR-300H and CR-450H in Figure 3) were associated with significant changes in their fractographs as illustrated in Figure 4c,d. In the CR-300H specimen, most SF zones were replaced by FF regions with parallel secondary cracks (Figure 4c). For the CR-450H specimen, the fractured surface was dominated by FF regions (Figure 4d) due to the high HE susceptibility.

Failure analyses of all fractured surfaces after tensile tests were performed using an SEM. Ductile dimple fracture was observed in all ordinary tensile specimens (not shown here). SEM fractographs of selected specimens after notched tensile tests are presented in Figure 5. The fracture modes of the CR-300 and CR-450 specimens differed slightly. In the CR-300 specimen, predominant fine shallow dimples mixed with sparsely flat cleavage-like fracture were observed within the FF zones ahead of notch front (Figure 5a). In contrast, mainly cleavage fracture with secondary cracks along austenite grain boundaries was found ahead of the notch front of the CR-450 specimen (Figure 5b), indicating the brittle nature of the sample. The CR-450 specimen, even without hydrogen-charging, was likely to suffer intergranular fracture under strain. Regarding the hydrogen-charged specimens, extensive cleavage-like fracture together with numerous secondary cracks was observed in the CR-300H specimen (Figure 5c), while the CR-450 specimen mainly exhibited intergranular fracture (Figure 5d).

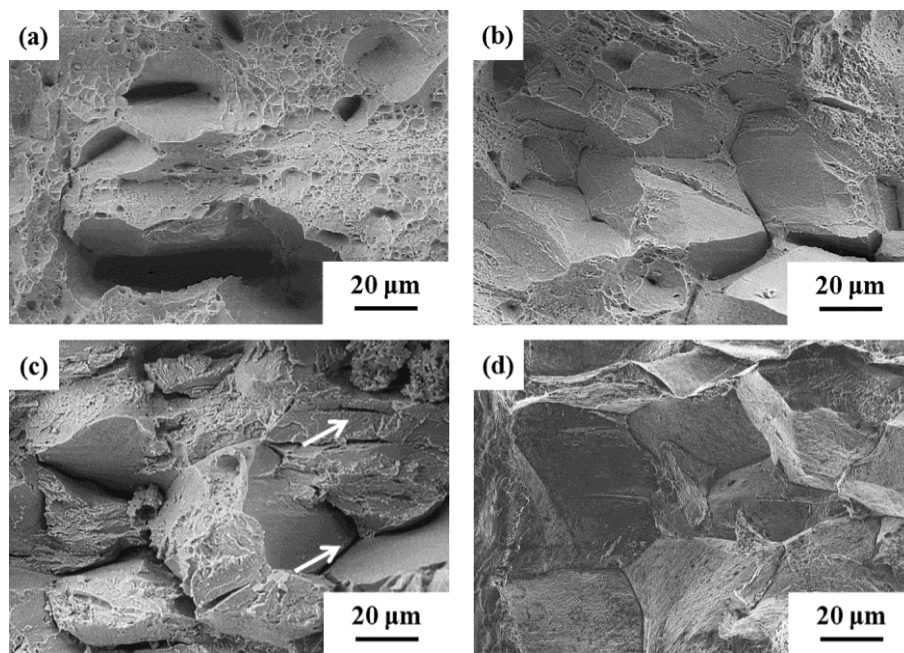


Figure 5. SEM fractographs of (a) CR-300, (b) CR-450, (c) CR-300H, and (d) CR-450H specimens after notched tensile test.

3.4. TEM Examinations

Figure 6 displays detailed TEM micrographs of the CR specimen. There were three distinct structures— ϵ -martensite, α' -martensite, and austenite—in the CR specimen. The microstructure of the CR specimen was primarily comprised of parallel strips of ϵ -martensite (hcp) in the austenite (γ , fcc) matrix, as illustrated in Figure 6a. The ϵ -martensite formed in slip bands due to the 30% cold rolling of the 301 SS. The α' -martensite (bcc) had also been found mainly at the intersections of ϵ -martensite strips. Similar results were obtained in prior study of the SCC of cold-rolled 304L SS [4,12], consistent with the location of α' -martensite, as shown in Figure 6b.

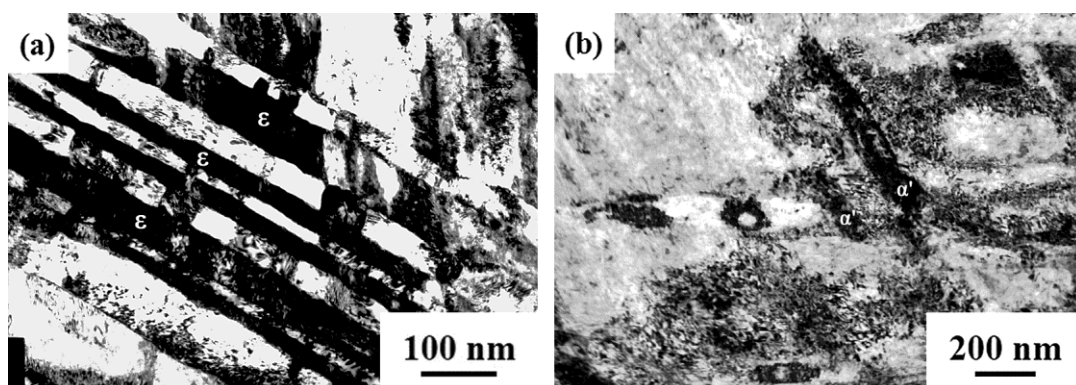


Figure 6. TEM micrographs of the CR specimen illustrating (a) ϵ -martensite strips in the austenite matrix, (b) α' -martensite at the intersections of ϵ -martensite strips.

In the CR-450 specimen, further aging at 450 °C for 160 h enhanced the transformation of metastable austenite into α' -martensite and the precipitation of $M_{23}C_6$ carbides along the grain boundaries, as displayed in Figure 7. In the CR and CR-300 specimens, the grain boundary α' -martensite and $M_{23}C_6$ carbides were not observed. Due to the presence of fresh grain boundary α' -martensite, the ferrite contents of the CR-450 specimen were higher than those of the CR and

CR-300 specimens. Both the precipitation of $M_{23}C_6$ carbides and increased α' -martensite along the grain boundaries resulted in increasing HE susceptibility of the CR-450H specimen, as compared with the CR-300H specimens. It was obvious that cold rolling the 301 SS induced partial austenite transformation into α' - and ε -martensite. The subsequent aging at 450 °C promoted the formation of grain boundary α' -martensite and $M_{23}C_6$ carbides, which were responsible for the low-temperature sensitization of the SS.

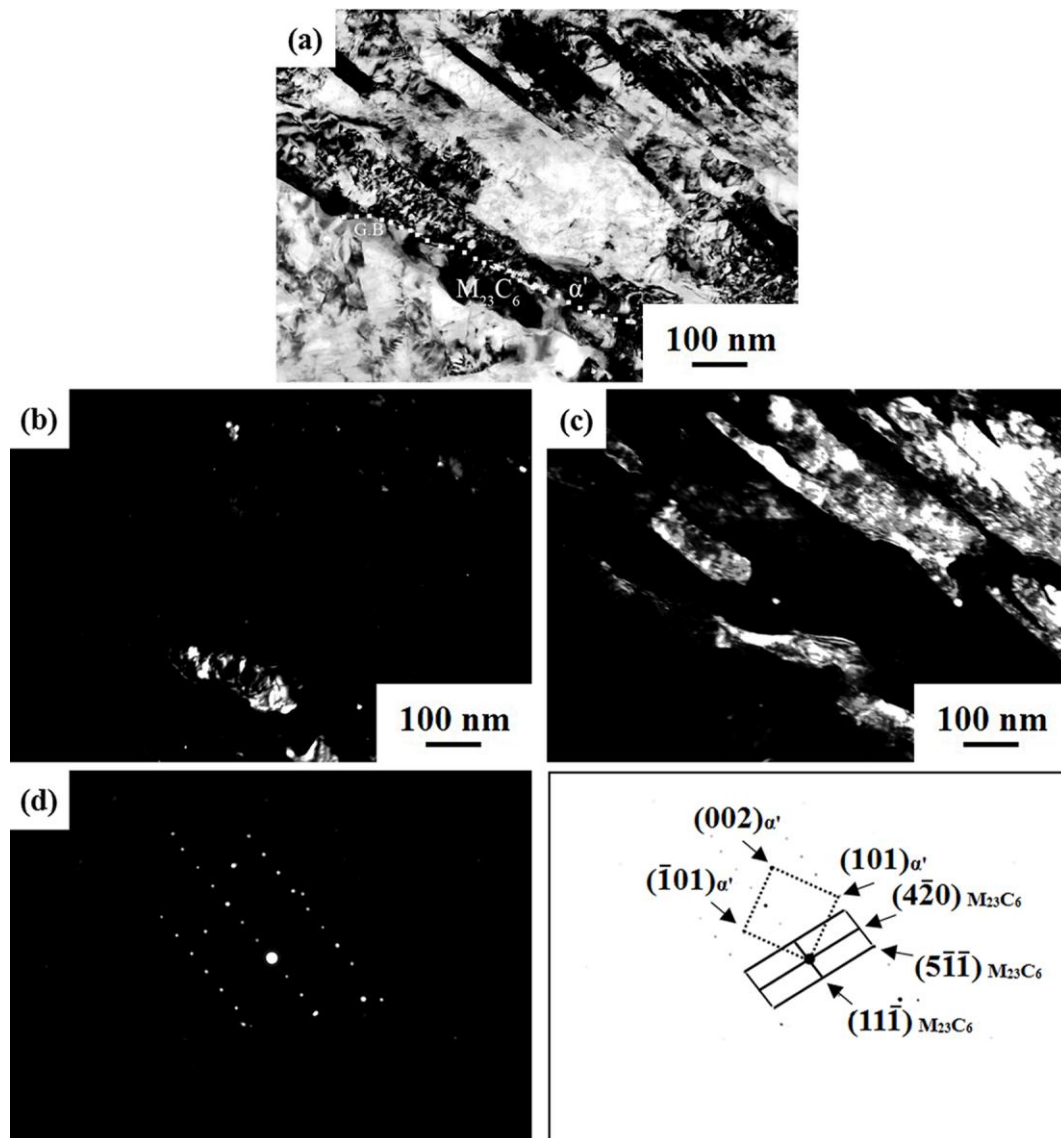


Figure 7. TEM images of the CR-450 specimen: (a) bright field image, (b) dark field image of carbides using $(11\bar{1})$ diffraction spot, (c) dark field image of α' martensite using $(\bar{1}01)$ spot, (d) selected area diffraction pattern with two identified structures.

Figure 8 shows TEM images of the G and σ phases in the CR-450 specimen. Nano-sized precipitates, G and σ phases, were found in the α' martensite of the CR-450 specimen, as shown in Figure 8a–c. The average size of the G phase precipitates was greater than that of the σ phase precipitates. The lattice image was transformed into a diffraction pattern by fast Fourier transform (FFT) for identification of the crystal structure of nano-sized precipitates by high resolution TEM. Figure 8b is a lattice image of the G phase formed in the α' matrix with a $[100]$ zone axis. A σ precipitate in the α' matrix with a $[013]$ zone axis is shown in Figure 8d.

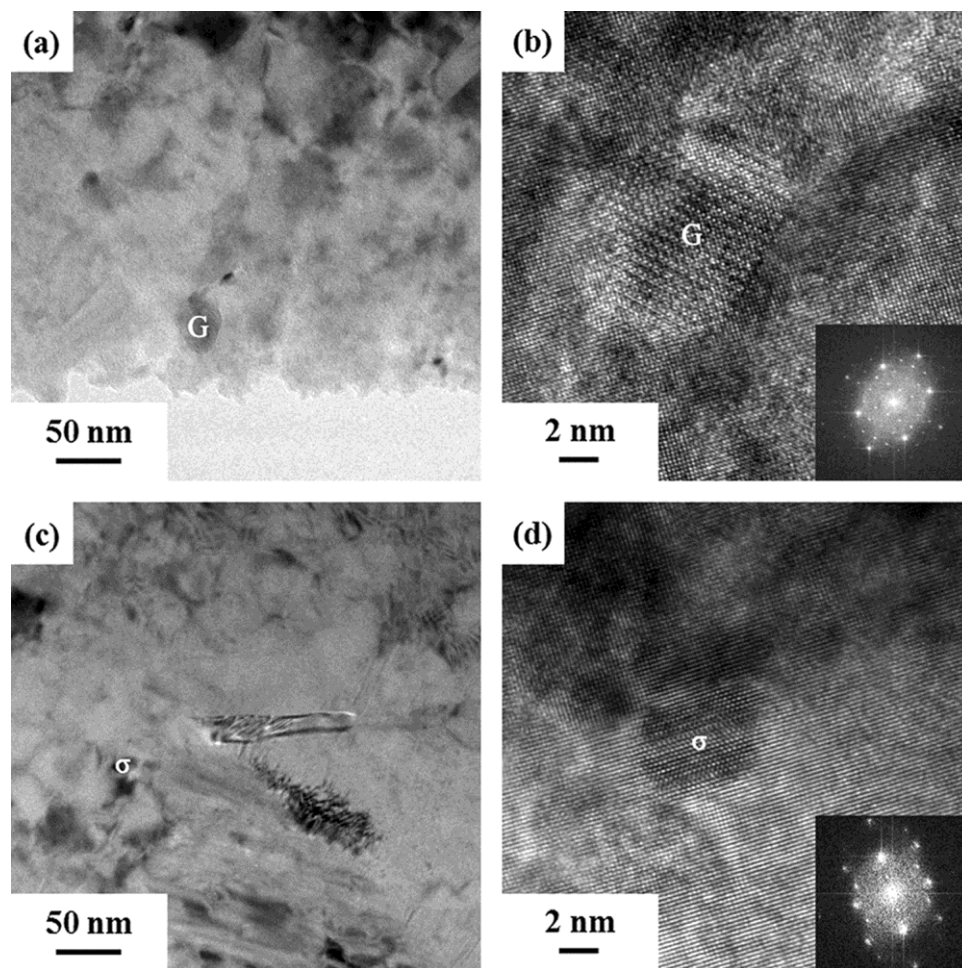


Figure 8. TEM images and high resolution lattice images with fast Fourier transform diffraction patterns of the CR-450 specimen: (a,b) G phase; and (c,d) σ phase.

4. Discussion

In general, an increase in annealing temperature reduces the strain-hardening effect of cold-rolled steels. Annealing treatment can improve the resistance of work-hardened steel to HE. As shown in Figure 6, cold work enhanced the formation of ε - and α' -martensite in the metastable austenitic SS. Moreover, metastable austenitic SSs undergo traditional sensitization when heated above 500 °C, and low-temperature sensitization occurs below 500 °C, if the cold work is applied. The formation of induced α' -martensite is responsible for its easy sensitization. In this work, aging the cold-rolled 301 SS at 450 °C (CR-450) assisted the formation of grain boundary α' -martensite and $M_{23}C_6$ carbides. In contrast, grain boundary α' -martensite and $M_{23}C_6$ carbides were not observed in the CR and CR-300 specimens.

As illustrated in Table 1, both UTS and YS of the CR-300 specimen were slightly higher than those of the CR one. In contrast, UTS and YS of the CR-450 specimen were obviously lower than those of CR and CR-300 ones. Moreover, all specimens showed equivalent tensile elongation tested in air. The results indicated increasing the annealing temperature to 450 °C did not improve the ductility but caused a decline in strength of the cold worked 301 SS. The results of notched tensile tests in air also revealed that the NTS of CR-450 specimen was lower than those of the others. As shown in Figure 4, the CR-450 specimen comprised of extensive flat fracture region (Figure 4b), in contrast, shear fracture dominated the fractographs of CR and CR-300 specimens (Figure 4a). It demonstrated the fact of high notch brittleness of the CR-450 specimen, and could be related to the brittle microstructures in

the specimen. SEM fractographs of the CR-450 specimen after the notched tensile test in air showed cleavage-like fracture along with intergranular fracture (Figure 5b), which could be associated with the formation of grain boundary α' -martensite and $M_{23}C_6$ carbides, as shown in Figure 7. Without the presence of brittle microstructures along grain boundaries, the notched fracture appearance of the CR and CR-300 specimens showed predominantly shallow dimple fracture (Figure 5a).

It was reported that the HE susceptibility of the austenitic SSs is affected by the compositions [35,36] and prestrained level of the SS [37,38]. Dynamic interactions between hydrogen and the induced martensite play important roles in the HE of the hydrogen-charged 304 SS [37]. The hydrogen enhances the formation of α' -martensite, which facilitates HE and dominates the fracture process of the metastable austenitic SS [7]. Moreover, the hydrogen source influences the location of crack initiation and propagation in austenitic SSs. An external hydrogen source promotes crack initiation and propagation at the surface. Similar to surface cracks, the propagation of internal cracks is accelerated by the presence of internal hydrogen in the 304 and 316 SSs [35].

In Table 1, both CR-300H and CR-450H specimens were highly susceptible to internal HE, especially for the CR-450H one. It was deduced that high sensitivity to HE of the cold worked 301 SS could be attributed to its low austenite stability under straining. The CR-450H specimen suffered from a greater loss of ductility than the CR-300H specimen, as displayed in Figure 3. Both macro- and micro-fractographs, as shown in Figures 4 and 5, also confirmed that the CR-450H specimen was more susceptible to internal HE than the CR-300H specimen. High extent of intergranular fracture in the CR-450H specimen was associated with the brittle characteristics of grain boundaries.

Nano-sized G and σ particles were observed in α' -martensite of CR-450 specimen (Figure 8). The precipitation of G phase in the ferrite matrix has also been reported in the duplex SS after prolonged aging above 350 °C [39]. The precipitation of nano-sized G and σ phases further strengthened the interiors of the grains of the CR-450 sample. The strengthening of the grain interior by nano-sized precipitates highlighted the weakness of the embrittled grain boundaries and favored crack propagation therein. Actually, hydrogen-charging caused more hydrogen to diffuse into the specimen at 450 °C than that at 300 °C. The hydrogen concentrations of the CR-300H and CR-450H were 12 and 20 ppm, respectively. A high hydrogen concentration is usually accompanied by high HE susceptibility. Both the deteriorated microstructure and the high hydrogen content accounted for the high HE susceptibility and extensive intergranular fracture of the CR-450H specimen.

5. Conclusions

The effects of cold rolling and subsequent hydrogen-charging at 300 °C or 450 °C for 160 h on the microstructure, tensile properties, and HE susceptibility of 301 SS were investigated. Cold rolling caused ϵ -martensite to form in parallel strips of the slip bands, and α' -martensite was found mainly at the intersections of ϵ -martensite. Hydrogen-charging at 300 °C and 450 °C led to severe HE of the cold-rolled 301 SS, particularly in the 450 °C charged specimens. In specimens that were not hydrogen-charged, the notched tensile fracture of the 450 °C-aged one showed brittle fracture appearance, which comprised of cleavage-like fracture together with intergranular separations. In the CR-450 specimen, α' -martensite and $M_{23}C_6$ carbides were formed along the grain boundary. Because of this fresh grain boundary of α' -martensite, the ferrite contents of the CR-450 specimen were higher than those of the CR and CR-300 specimens. Moreover, very fine precipitates including the G and σ phases were found in the α' -martensite. The formation of grain boundary α' -martensite and $M_{23}C_6$ carbides together with nano-sized precipitates in the α' -martensite were responsible for the high HE susceptibility and low-temperature sensitization of the CR-450 specimen. In contrast, those of grain boundary precipitates and nano-sized phases were not observed in the CR and CR-300 specimens.

Acknowledgments: The authors gratefully acknowledge the partial financial support of this research by the National Science Council, Republic of China, Taiwan.

Author Contributions: L.W. Tsay and R.K. Shiue designed and planned the experiment. C. Chen contributed to the discussion of the results. C. Yu performed the tests and TEM examinations. All co-authors contributed to the manuscript proof and submissions.

Conflicts of Interest: The authors declare no conflict of interest.

References

1. Böhner, A.; Niendorf, T.; Amberger, D.; Höppel, H.W.; Göken, M.; Maier, H.J. Martensitic transformation in ultrafine-grained stainless steel AISI 304L under monotonic and cyclic loading. *Metals* **2012**, *2*, 56–64. [[CrossRef](#)]
2. Michler, T.; Naumann, J. Microstructural aspects upon hydrogen environment embrittlement of various bcc steels. *Int. J. Hydro. Energy* **2010**, *35*, 821–832. [[CrossRef](#)]
3. Michler, T.; Naumann, J.; Hock, M.; Berreth, K.; Balogh, M.P.; Sattler, E. Microstructural properties controlling hydrogen environment embrittlement of cold worked 316 type austenitic stainless steels. *Mater. Sci. Eng. A* **2015**, *628*, 252–261. [[CrossRef](#)]
4. Gey, N.; Petit, B.; Humbert, M. Electron backscattered diffraction study of ϵ/α' martensitic variants induced by plastic deformation in 304 stainless steel. *Metall. Mater. Trans. A* **2005**, *36*, 3291–3299. [[CrossRef](#)]
5. Bak, S.; Abro, M.; Lee, D. Effect of hydrogen and strain-induced martensite on mechanical properties of AISI 304 stainless steel. *Metals* **2016**, *6*, 169. [[CrossRef](#)]
6. Pan, C.; Chu, W.Y.; Li, Z.B.; Liang, D.T.; Su, Y.J.; Gao, K.W.; Qiao, L.J. Hydrogen embrittlement induced by atomic hydrogen and hydrogen-induced martensites in type 304L stainless steel. *Mater. Sci. Eng. A* **2003**, *351*, 293–298. [[CrossRef](#)]
7. Lai, C.L.; Tsay, L.W.; Chen, C. Effect of microstructure on hydrogen embrittlement of various stainless steels. *Mater. Sci. Eng. A* **2013**, *584*, 14–20. [[CrossRef](#)]
8. Mine, Y.; Narazaki, C.; Murakami, K.; Matsuoka, S.; Murakami, Y. Hydrogen transport in solution-treated and pre-strained austenitic stainless steels and its role in hydrogen-enhanced fatigue crack growth. *Int. J. Hydro. Energy* **2009**, *34*, 1097–1107. [[CrossRef](#)]
9. Alyousif, O.M.; Nishimura, R. Stress corrosion cracking and hydrogen embrittlement of sensitized austenitic stainless steels in boiling saturated magnesium chloride solutions. *Corros. Sci.* **2008**, *50*, 2353–2359. [[CrossRef](#)]
10. Alyousif, O.M.; Nishimura, R. The stress corrosion cracking behavior of austenitic stainless steels in boiling magnesium chloride solutions. *Corros. Sci.* **2007**, *49*, 3040–3051. [[CrossRef](#)]
11. Alyousif, O.M.; Nishimura, R. The effect of test temperature on SCC behavior of austenitic stainless steels in boiling saturated magnesium chloride solution. *Corros. Sci.* **2006**, *48*, 4283–4293. [[CrossRef](#)]
12. Lai, C.L.; Tsay, L.W.; Kai, W.; Chen, C. Notched tensile tests of cold-rolled 304L stainless steel in 40 wt. % 80 °C MgCl₂ solution. *Corros. Sci.* **2009**, *51*, 380–386. [[CrossRef](#)]
13. Lai, C.L.; Tsay, L.W.; Kai, W.; Chen, C. The effects of cold rolling and sensitisation on hydrogen embrittlement of AISI 304L welds. *Corros. Sci.* **2010**, *52*, 1187–1193. [[CrossRef](#)]
14. Li, W.J.; Young, M.C.; Lai, C.L.; Kai, W.; Tsay, L.W. The effects of rolling and sensitization treatments on the stress corrosion cracking of 304L stainless steel in salt-spray environment. *Corros. Sci.* **2013**, *68*, 25–33. [[CrossRef](#)]
15. Raman, R.; Siew, W. Stress corrosion cracking of an austenitic stainless steel in nitrite-containing chloride solutions. *Materials* **2014**, *7*, 7799–7808. [[CrossRef](#)]
16. García, C.; Martín, F.; Tiedra, P.D.; Heredero, J.A.; Aparicio, M.L. Effects of prior cold work and sensitization heat treatment on chloride stress corrosion cracking in type 304 stainless steels. *Corros. Sci.* **2001**, *43*, 1519–1539. [[CrossRef](#)]
17. García, C.; Martín, F.; de Tiedra, P.; Alonso, S.; Aparicio, M.L. Stress corrosion cracking behavior of cold-worked and sensitized type 304 stainless steel using the slow strain rate test. *Corros. Sci.* **2002**, *58*, 849–857. [[CrossRef](#)]
18. Ghosh, S.; Kain, V. Effect of surface machining and cold working on the ambient temperature chloride stress corrosion cracking susceptibility of AISI 304L stainless steel. *Mater. Sci. Eng. A* **2010**, *527*, 679–683. [[CrossRef](#)]
19. Ghosh, S.; Kain, V. Microstructural changes in aisi 304L stainless steel due to surface machining: Effect on its susceptibility to chloride stress corrosion cracking. *J. Nucl. Mater.* **2010**, *403*, 62–67. [[CrossRef](#)]

20. Martin, M.; Weber, S.; Izawa, C.; Wagner, S.; Pundt, A.; Theisen, W. Influence of machining-induced martensite on hydrogen-assisted fracture of AISI type 304 austenitic stainless steel. *Int. J. Hydro. Energy* **2011**, *36*, 11195–11206. [[CrossRef](#)]
21. Domankova, M.; Marek, P.; Magula, V. Effect of deformation and heat treatment on grain boundary sensitization in austenitic stainless steels. *Metal* **2006**, *23*.
22. Nasreldin, A.M.; Gad, M.M.A.; Hassan, I.T.; Ghoniem, M.M.; El-sayed, A.A. Effect of hydrogen charging on the tensile and constant load properties of an austenitic stainless steel weldment. *J. Mater. Sci. Technol.* **2001**, *17*, 444–448.
23. Parvathavarthini, N.; Dayal, R.K. Influence of chemical composition, prior deformation and prolonged thermal aging on the sensitization characteristics of austenitic stainless steels. *J. Nucl. Mater.* **2002**, *305*, 209–219. [[CrossRef](#)]
24. Silva, M.J.G.; Souza, A.A.; Sobral, A.V.C.; de Lima-Neto, P.; Abreu, H.F.G. Microstructural and electrochemical characterization of the low-temperature sensitization of AISI 321 stainless steel tube used in petroleum refining plants. *J. Mater. Sci.* **2003**, *38*, 1007–1011. [[CrossRef](#)]
25. Singh, R. Influence of cold rolling on sensitization and intergranular stress corrosion cracking of AISI 304 aged at 500 °C. *J. Mater. Process. Technol.* **2008**, *206*, 286–293. [[CrossRef](#)]
26. Prasanthi, T.N.; Sudha, C.; Parameswaran, P.; Punniyamoorthy, R.; Chandramouli, S.; Saroja, S.; Rajan, K.K.; Vijayalakshmi, M. Failure analysis of a 304 steel component aged at 623 K. *Eng. Fail. Anal.* **2013**, *31*, 28–39. [[CrossRef](#)]
27. Lv, J.; Luo, H. Temperature dependence of sensitization on tensile pre-strained AISI 304 stainless steels. *J. Alloy. Compd.* **2014**, *588*, 509–513.
28. Kain, V.; Chandra, K.; Adhe, K.N.; De, P.K. Effect of cold work on low-temperature sensitization behaviour of austenitic stainless steels. *J. Nucl. Mater.* **2004**, *334*, 115–132. [[CrossRef](#)]
29. Han, G.; He, J.; Fukuyama, S.; Yokogawa, K. Effect of strain-induced martensite on hydrogen environment embrittlement of sensitized austenitic stainless steels at low temperatures. *Acta Mater.* **1998**, *46*, 4559–4570. [[CrossRef](#)]
30. Talonen, J.; Hänninen, H. Formation of shear bands and strain-induced martensite during plastic deformation of metastable austenitic stainless steels. *Acta Mater.* **2007**, *55*, 6108–6118. [[CrossRef](#)]
31. Talonen, J.; Aspegren, P.; Hänninen, H.J. Comparison of different methods for measuring strain induced α' -martensite content in austenitic steels. *Mater. Sci. Technol.* **2004**, *20*, 1506–1512.
32. Yokobori, A.T.; Nemoto, T.; Satoh, K.; Yamada, T. Numerical analysis on hydrogen diffusion and concentration in solid with emission around the crack tip. *Eng. Fract. Mech.* **1996**, *55*, 47–60. [[CrossRef](#)]
33. Hardie, D.; Liu, S.E. The effect of stress concentration on hydrogen embrittlement of a low alloy steel. *Corros. Sci.* **1996**, *38*, 721–733. [[CrossRef](#)]
34. Liu, S.E.; Ziyong, Z.; Wei, K. Notch severity effect on hydrogen embrittlement of type 4340 steel. *J. Mater. Sci. Technol.* **1996**, *12*, 51–56.
35. San Marchi, C.; Michler, T.; Nibur, K.A.; Somerday, B.P. On the physical differences between tensile testing of type 304 and 316 austenitic stainless steels with internal hydrogen and in external hydrogen. *Int. J. Hydro. Energy* **2010**, *35*, 9736–9745. [[CrossRef](#)]
36. Neuharth, J.J.; Cavalli, M.N. Investigation of high-temperature hydrogen embrittlement of sensitized austenitic stainless steels. *Eng. Fail. Anal.* **2015**, *49*, 49–56. [[CrossRef](#)]
37. Yoshioka, Y.; Yokoyama, K.I.; Sakai, J.I. Role of dynamic interactions between hydrogen and strain-induced martensite transformation in hydrogen embrittlement of type 304 stainless steel. *ISIJ Int.* **2015**, *55*, 1772–1780. [[CrossRef](#)]
38. Matsuo, T.; Yamabe, J.; Matsuoka, S. Effects of hydrogen on tensile properties and fracture surface morphologies of type 316L stainless steel. *Int. J. Hydro. Energy* **2014**, *39*, 3542–3551. [[CrossRef](#)]
39. Lo, K.H.; Lai, J.K.L. Microstructural characterization and change in a.c. magnetic susceptibility of duplex stainless steel during spinodal decomposition. *J. Nucl. Mater.* **2010**, *401*, 143–148. [[CrossRef](#)]

